In-plane magnetization effect on current-induced spin-orbit torque in a ferromagnet/topological insulator bilayer with hexagonal warping

Jia-Yu Li, Rui-Qiang Wang,* Ming-Xun Deng,† and Mou Yang
Guangdong Provincial Key Laboratory of Quantum Engineering and Quantum Materials, School of Physics and Telecommunication Engineering, South China Normal University, Guangzhou 510006, China

(Received 21 December 2018; revised manuscript received 18 March 2019; published 22 April 2019)

Current-induced spin polarization and the resulting spin-orbit torque (SOT) in a ferromagnet/topological insulator (FM/TI) bilayer have been investigated by taking into account the hexagonal warping spectrum of topological surface states. We find that the usually ignored in-plane FM magnetization plays an important role to the spin polarization. The resulting spin polarization and spin torque significantly depend on azimuthal angle of the magnetization, which has not been reported theoretically before in the linear dispersion TI model. These interesting results arise from the combination effect of in-plane magnetization and warping effect by modifying the Berry curvature and impurity scattering. Based on Matsubara-Green function approach, we derive the formula of SOT and analyze the results analytically and numerically, including the contribution from intrabands and interbands, and intrinsic and extrinsic contribution. More importantly, it is found that the hexagonal warping can prominently enhance the antidamping SOT if there exists the in-plane FM magnetization, which provides a new perspective to understand the recent giant SOT effect.

DOI: 10.1103/PhysRevB.99.155139

I. INTRODUCTION

The existing technology on magnetoresistive random-access memory through the spin transfer torque meets the bottleneck for high current density requirement in a ferromagnet/insulator/ferromagnet (FM/I/FM) biheterostructure [1,2]. An alternative mechanism, based on the electrically controlled spin-orbit torque (SOT), is proposed to circumvent this issue, which is realized even in the simple single heterostructure of FM/spin-orbit interaction (SOI) materials and has been substantially investigated recently [3–5]. When charge current passes the SOI system, the nonequilibrium spin polarization of conducting electrons is induced owing to the transfer of orbit-to-spin angular momentum, and in turn this spin polarization exerts a spin torque on the local magnetization of the adjacent ferromagnetic layer [6,7] and even the antiferromagnetic layer [8,9]. The SOT effect in the FM/heavy metal heterostructures with Rashba SOI generated from the inversion symmetry breaking [10–18] has received great attention.

Topological surface states [19,20] with spin-momentum locking endow topological insulators (TIs) with potential applications in spintronic devices. Compared with FM/heavy metal heterostructure, FM/TI heterostructure can reach the perfect spin polarization when Dirac fermions flow on the surface of TI because of strong spin-orbit coupling. Recent experiments in FM/TI layered structure reported larger intrinsic SOT field [21–25] and even a giant SOT [26–29] which is by several orders of magnitude larger than any other material. Ferromagnetic resonance measurements in a TI interfaced with FM showed an exceptionally large spin conversion efficiency [26]. With these exciting breakthroughs made continually in experiments, however, the underlying microscopic origin of SOT remains under debate. A general viewpoint is that dampinglike SOT (DL-SOT) is attributed to the spin Hall effect (SHE) from bulk bands [2,30], and the fieldlike SOT (FL-SOT) is from the inverse spin galvanic effect [31–33] in the interface. Nevertheless, recent experiments [27,34] observed a giant antidampinglike torque that cannot be ascribed to the bulk SHE but to a scattering-independent origin in the Berry curvature of the band structure, challenging the existing theoretical mechanisms. Also, TIs [26] were reported to generate both the in-plane and out-of-plane SOTs with the same order, which is unexpected from the usual spin-momentum locking argument. Theoretically, Li *et al.* [35] addressed that the contribution of interband mixing to the SOT presents an outstanding opportunity to explain the emergence of large antidampinglike torques that cannot be readily attributed to the SHE.

In fact, the FM magnetization and spin polarization of Dirac electrons in FM/TI heterostructure interplay with each other and so the SOT will exhibit a complex dependence on the magnetization direction due to the distortion of the band structure. One can notice that in FM/TI heterostructure [33,36–38], the SOT can be expressed in a general form $\tau = \tau_f \mathbf{m}\times\mathbf{y} + \tau_d m_z \mathbf{m}\times e\mathbf{E}$, where $\mathbf{y} = \hat{z}\times e\mathbf{E}$, and $\tau_f(\tau_d)$ stands for the strength of the FL-SOT (DL-SOT). Obviously, this DL-SOT vanishes if $m_z = 0$ while the magnetization m_x and m_y lying in the plane of the surface has no effect on the polarized field $\delta\mathbf{S}$, which is defined by $\tau = \frac{2J}{\hbar}\mathbf{m}\times\delta\mathbf{S}$ with J being the magnetic exchange energy between the spin of conducting electrons and the FM layer. Compared with the bulk SHE-induced torque [35,39,40], where $\tau = \tau_f \mathbf{m}\times\mathbf{y} + \tau_d \mathbf{m}\times[\mathbf{y}\times\mathbf{m}]$, the TIs are lacking the term of $m_x \mathbf{m}\times\hat{z}$,

*wangruiqiang@m.scnu.edu.cn
†dengmingxun@scnu.edu.cn

contributed by in-plane m_x. Nevertheless, in many recent experiments on the ferromagnetic resonance [22,26,41], the in-plane magnetic field is extensively applied and so the in-plane magnetization of FM is unavoidable. Experimental measurements in the TI bilayer [22,26] also observed complex SOT phenomenology since the polarized field $\delta\mathbf{S}$ depends on the azimuthal angle of $\mathbf{m}$, which is often not captured by the above physical scenarios. Theoretically, as far as we know, there is no theoretical study on the role of in-plane magnetization on the spin torque in FM/TI layered structure.

In previous works on SOT in FM/TI heterostructure [33,37,38], the linear dispersion of TIs was employed, where the in-plane FM magnetization can be straightforwardly eliminated by a scaled transform. But in the high energy regime which is usually the work regime to generate the current-induced torque, the in-plane magnetization will play an important role due to the existence of the warping effect. In this work, we extend the previous discussions further to the more realistic case beyond the linear dispersion by taking into account high order hexagonal warping and investigate the magnetic dynamics associated with spin-momentum locking surface states. The hexagonal warping in the band structure [42,43] of the Dirac cone arises when we take into account the next-order terms in the dispersion of TIs with the hexagonal lattices [44,45], such as Bi_2Te_3 and Bi_2Se_3. Recently, it is found that the warping effect significantly modifies the transport properties, such as dc conductivity [46,47] and optical conductivity [48–50].

In this paper, we in detail analyze how the SOT is influenced by in-plane FM magnetization analytically and numerically, including the intrinsic and extrinsic contributions and interband and intraband contributions. It is found that the hexagonal warping along with the in-plane magnetization can enhance the antidampinglike SOT and make the SOT significantly depend on the azimuthal angle of magnetization.

II. THEORETICAL MODEL AND METHOD

We consider a three-dimensional (3D) TI surface with hexagonal warping spectrum covered by an FM, as shown in Fig. 1. Near the Dirac point in the surface Brillouin zone of the TIs, the low-energy effective Hamiltonian [44,51] reads

$$H_{\rm TI} = \sum_{\mathbf{k}} c^\dagger_{\mathbf{k}}\Big[\hbar v_F(\sigma\times\mathbf{k})\cdot\hat{z} + \frac{\lambda}{2}(k_+^3 + k_-^3)\sigma_z + J\mathbf{m}\cdot\boldsymbol{\sigma}\Big]c_{\mathbf{k}}, \tag{1}$$

where $c_{\mathbf{k}} = (c_{\mathbf{k}\uparrow}, c_{\mathbf{k}\downarrow})^T$, $\mathbf{k} = (k_x, k_y, 0)$ is the in-plane wave vector, $\boldsymbol{\sigma} = (\sigma_x, \sigma_y, \sigma_z)$ is the vector of three Pauli matrices acting on the real spin, $\hat{z}$ is the direction vector normal to the TI plane, and $k_\pm = k_x \pm ik_y$. The first term is the Rashba-type spin-orbit coupling with a Fermi velocity v_F. The warping parameter λ in the second term characterizes the hexagonal warping effect of 3D-TI. The last term in the above Hamiltonian stands for the magnetic exchange interaction between the spin $\boldsymbol{\sigma}$ of conducting electrons and the FM layer whose unit vector of the magnetization is $\mathbf{m} = (m_x, m_y, m_z) = (\sin\theta_m\cos\phi_m, \sin\theta_m\sin\phi_m, \cos\theta_m)$, as shown in Fig. 1(a). The dispersion relation of the model Hamiltonian is

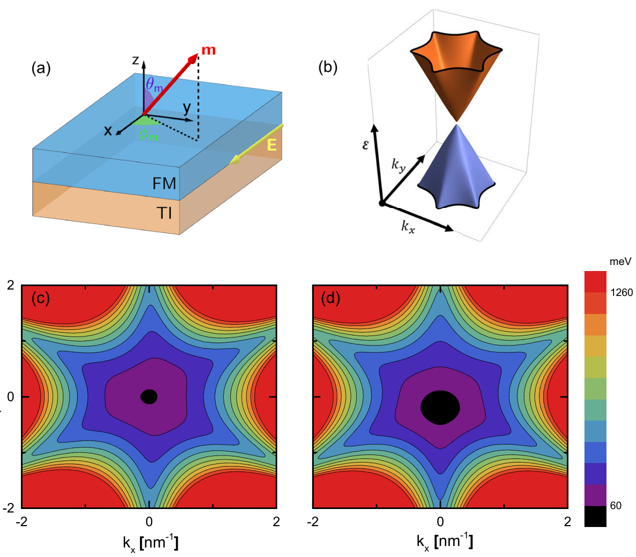

FIG. 1. Schematic (a) and band structure (b) of the proposed FM/TI model. Anisotropic energy contours of $\varepsilon_{\mathbf{k}}$ for (c) $\mathbf{m}\parallel\hat{z}$ and (d) $\mathbf{m}\parallel\hat{x}$. Parameters: $\hbar v_F = 0.255$ eV nm [44], $\lambda = 250$ eV Å^3 [51], and $J = 0.05$ eV.

$\varepsilon_{\mathbf{k}\pm} = \pm\varepsilon_{\mathbf{k}}$ with

$$\varepsilon_{\mathbf{k}} = \sqrt{\hbar^2 v_F^2 k^2 + 2J\hbar v_F(\mathbf{m}\times\mathbf{k})\cdot\hat{z} + J^2 m_\parallel^2 + \Delta_{\mathbf{k}}^2}, \tag{2}$$

where $m_\parallel^2 = m_x^2 + m_y^2$, $\Delta_{\mathbf{k}} = \lambda k_x(k_x^2 - 3k_y^2) + Jm_z$, and $\pm$ label the conduction and valence bands, respectively.

Without the warping effect $\lambda = 0$, the energy band is gapped to be $\varepsilon_g = 2Jm_z$ by the out-of-plane magnetization while the in-plane magnetization only shifts the Dirac cone to $(Jm_y/\hbar v_F, -Jm_x/\hbar v_F)$ in momentum space. By redefining the position of the Dirac node, these in-plane magnetization components are not expected to impact any physical observables. In fact, we can eliminate the in-plane magnetization components by performing a gauge transformation in the electron field operators [52] $c_{\mathbf{k}} \to c_{\mathbf{k}}\exp[-\frac{i}{\hbar}e\mathbf{A}\cdot\mathbf{k}]$ with $e\mathbf{A} = \frac{J}{\hbar v_F}(\hat{z}\times\mathbf{m})$. For a finite λ, however, the gauge symmetry is broken since the in-plane momentum is cubic dependent in $\Delta_{\mathbf{k}}$. As a consequence, an extra energy gap $\varepsilon_g' = -2\lambda(\frac{J}{\hbar v_F})^3\sin^3\theta_m\sin(3\phi_m)$, opened at the Dirac point, is induced by the in-plane magnetization. As the TIs is covered by a FM, the snowflake energy structure is disturbed not only by the out-of-plane magnetization m_z but also by the in-plane component $m_{x/y}$, as depicted in Figs. 1(c) and 1(d). One can notice that ε_g' can have the opposite sign to ε_g and so the competition of the contribution between the exchange energy J and the warping parameter λ leads to the complicated anisotropy in the band structure and in turn significantly affects the Berry curvature.

The eigenstates of the Hamiltonian Eq. (1) can be solved as

$$|u_+\rangle = \begin{pmatrix}\cos\frac{\zeta}{2}\\ e^{i\eta}\sin\frac{\zeta}{2}\end{pmatrix},\quad |u_-\rangle = \begin{pmatrix}-\sin\frac{\zeta}{2}\\ e^{i\eta}\cos\frac{\zeta}{2}\end{pmatrix}, \tag{3}$$

where $\cos\zeta = \frac{\Delta_{\mathbf{k}}}{\varepsilon_{\mathbf{k}}}$ and $\tan\eta = \frac{Jm_y - \hbar v_F k_x}{Jm_x + \hbar v_F k_y}$. According to the definition of Berry curvature of energy bands

$\mathbf{\Omega}^{\pm} = i\nabla_{\mathbf{k}} \times \langle u_{\pm}|\nabla_{\mathbf{k}}|u_{\pm}\rangle$, we derive it as

$$\Omega_z^{\pm} = \mp\frac{\hbar v_F}{2\varepsilon_{\mathbf{k}}^3}\{\hbar v_F J m_z - 2\lambda\hbar v_F k^3\cos(3\phi_k) + 3\lambda J k^2[m_x\sin(2\phi_k) + m_y\cos(2\phi_k)]\}, \tag{4}$$

with $\phi_k = \arctan(k_y/k_x)$. Not only m_z but $m_{x/y}$ is involved in the Berry curvature for hexagonal warping bands. Thus, it is expected that the in-plane magnetization will contribute to the intrinsic SOT.

Below, we first present a theoretical method based on the Matsubara-Green function formalism to derive a general formula for the nonequilibrium spin polarization induced by an external electric field. To describe the interaction between the conducting electron and the electric field, one can introduce a time-dependent vector potential $\mathbf{A}(t) = \mathbf{A}(\Omega)e^{-i\Omega t/\hbar}$ with frequency Ω . The electric field is described by $\mathbf{E}(t) = -\partial_t\mathbf{A}(t) = -\frac{i\Omega}{\hbar}\mathbf{A}(t)$. Thus, a perturbation term in the form of $H_p(t) = -\mathbf{j}\cdot\mathbf{A}(t)$ is added to H_{TI} in Eq. (1). According to the linear response theory [37,53], the spin polarization induced by the electric perturbation can be calculated as

$$\delta\mathbf{S} = -\lim_{\Omega\to 0}\frac{1}{\Omega}\mathrm{Im}\Pi_{\mathbf{s},\mathbf{j}}(i\Omega_n \to \Omega + i0^+). \tag{5}$$

Here, $\Pi_{\mathbf{s},\mathbf{j}}(i\Omega) = \frac{1}{\beta}\int_0^\beta d\tau e^{\frac{i}{\hbar}\Omega\tau}\langle T_\tau \mathbf{s}(\tau)(\mathbf{j}(0)\cdot\mathbf{E})\rangle$ is the imaginary-time retarded correlation function between conducting electron spin $\mathbf{s} = \frac{\hbar}{2}\boldsymbol{\sigma}$ and current operator $\mathbf{j}$, and $\beta = 1/k_{\mathrm{B}}T$ and T_τ is the time order operator. Defining the Green's function $G_{\mathbf{k}}(\tau) = -i\langle T_\tau c_{\mathbf{k}}(\tau)c_{\mathbf{k}}^\dagger(0)\rangle$, one can find

$$\Pi_{\mathbf{s},\mathbf{j}}(i\Omega) = \frac{1}{V\beta}\sum_{\mathbf{k},m}\mathrm{Tr}[\mathbf{s}G_{\mathbf{k}}(i\omega_m + i\Omega)(\mathbf{j}\cdot\mathbf{E})G_{\mathbf{k}}(i\omega_m)], \tag{6}$$

where V is the area of topological surface and the current operator is $\mathbf{j} = e\mathbf{v}$ with the velocity operator $\mathbf{v} = \frac{1}{\hbar}\nabla_{\mathbf{k}}H_{\mathrm{TI}}$.

Performing the standard procedure on analytical continuation of the Matsubara-Green function [54], we reach

$$\begin{aligned}\Pi_{\mathbf{s},\mathbf{j}}(\Omega) &= \sum_{\mathbf{k}}\int d\varepsilon f(\varepsilon)\mathrm{Tr}\big\{\mathbf{s}\big[G_{\mathbf{k}}^R(\varepsilon) - G_{\mathbf{k}}^A(\varepsilon)\big](\mathbf{j}\cdot\mathbf{E})G_{\mathbf{k}}^A(\varepsilon - \Omega)\\ &\quad + \mathbf{s}G_{\mathbf{k}}^R(\varepsilon + \Omega)(\mathbf{j}\cdot\mathbf{E})\big[G_{\mathbf{k}}^R(\varepsilon) - G_{\mathbf{k}}^A(\varepsilon)\big]\big\}.\end{aligned} \tag{7}$$

Here, $f(\varepsilon) = [e^{\beta(\varepsilon-\mu_F)} + 1]^{-1}$ is the Fermi-Dirac distribution function and $G_{\mathbf{k}}^{R/A}(\varepsilon)$ is the retarded/advanced Green's function with respect to H_{TI}. The Green function matrix $G_{\mathbf{k}}^{R/A}(\varepsilon)$ can be obtained from the eigenstates Eq. (3)

$$G_{\mathbf{k}}^{R/A}(\varepsilon) = \sum_{\nu=\pm}\frac{|u_\nu\rangle\langle u_\nu|}{\varepsilon - \varepsilon_{\mathbf{k}\nu} \pm i\Gamma}, \tag{8}$$

where the weak impurity effect, for convenience, is taken into account with a spin-independent finite imaginary part Γ. In Eq. (8), we divide the Green function into different bands, which is convenient to discuss the contribution from intrabands and interbands.

From the above derivation, one can clearly see that the warping parameter λ affects the correlation function $\Pi_{\mathbf{s},\mathbf{j}}(\Omega)$ by entering both the Green's functions and current operator. If proceeding an integration by parts in Eq. (7) and inserting $\Pi_{\mathbf{s},\mathbf{j}}(\Omega)$ into Eq. (5), one in the dc limit $\Omega \to 0$ can obtain the Streda-Smrcka version of the Kubo formula for $\delta\mathbf{S}$, resembling the formula of universally adopted electric conductivity [55–57], which consists of two parts:

$$\delta\mathbf{S}^{\mathrm{sur}} = \frac{\hbar e}{2\pi V}\mathrm{Re}\sum_{\mathbf{k}}\int d\varepsilon\partial_\varepsilon f(\varepsilon) \times \mathrm{Tr}\big\{\mathbf{s}G_{\mathbf{k}}^R(\varepsilon)(\mathbf{v}\cdot\mathbf{E})\big[G_{\mathbf{k}}^R(\varepsilon) - G_{\mathbf{k}}^A(\varepsilon)\big]\big\}, \tag{9}$$

$$\delta\mathbf{S}^{\mathrm{sea}} = \frac{\hbar e}{2\pi V}\mathrm{Re}\sum_{\mathbf{k}}\int d\varepsilon f(\varepsilon)\mathrm{Tr}\big\{\mathbf{s}G_{\mathbf{k}}^R(\varepsilon)(\mathbf{v}\cdot\mathbf{E})\partial_\varepsilon G_{\mathbf{k}}^R(\varepsilon) - \mathbf{s}\partial_\varepsilon G_{\mathbf{k}}^R(\varepsilon)(\mathbf{v}\cdot\mathbf{E})G_{\mathbf{k}}^R(\varepsilon)\big\}. \tag{10}$$

$\delta\mathbf{S}^{\mathrm{sur}}$ originates from the contribution of Fermi surface characterized by $\partial_\varepsilon f(\varepsilon)$ while $\delta\mathbf{S}^{\mathrm{sea}}$ comes from the Fermi sea characterized by $f(\varepsilon)$. In this study, we are interested in the current-induced torque and so keep $|\mu_F| > |\varepsilon_g + \varepsilon_g'|/2$, where the contribution from the Fermi sea can be ignored safely [37]. Substituting the expressions of $G_{\mathbf{k}}^{R/A}(\varepsilon)$ into Eq. (9) and taking $\partial_\varepsilon f(\varepsilon) \to -\delta(\mu_F - \varepsilon)$ at low temperatures, we obtain

$$\begin{aligned}\delta\mathbf{S} &= -\frac{\hbar e}{2\pi V}\mathrm{Re}\sum_{\mathbf{k}}\mathrm{Tr}\big\{\mathbf{s}G_{\mathbf{k}}^R(\mu_F)(\mathbf{v}\cdot\mathbf{E})G_{\mathbf{k}}^A(\mu_F)\big\}\\ &= \frac{\hbar e}{2\pi V}\mathrm{Re}\sum_{\mathbf{k},\nu\xi}\frac{\langle\mathbf{s}\rangle_{\nu\xi}}{\mu_F - \varepsilon_{\mathbf{k}\xi} + i\Gamma}\frac{\langle\mathbf{v}\cdot\mathbf{E}\rangle_{\xi\nu}}{\mu_F - \varepsilon_{\mathbf{k}\nu} - i\Gamma},\end{aligned} \tag{11}$$

where $\langle\mathbf{O}\rangle_{\nu\xi} = \langle u_\nu|\mathbf{O}|u_\xi\rangle$. The spin polarization can be separated into three parts: $\delta\mathbf{S} = \delta\mathbf{S}^{\mathrm{intra}} + \delta\mathbf{S}^{\mathrm{inter},1} + \delta\mathbf{S}^{\mathrm{inter},2}$, with the intraband contribution

$$\delta\mathbf{S}^{\mathrm{intra}} = \frac{e\hbar}{2\Gamma V}\mathrm{Re}\sum_{\mathbf{k},\nu}\langle\mathbf{s}\rangle_{\nu\nu}\langle\mathbf{v}\cdot\mathbf{E}\rangle_{\nu\nu}\delta(\mu_F - \varepsilon_{\mathbf{k}\nu}), \tag{12}$$

and the interband contributions

$$\delta\mathbf{S}^{\mathrm{inter},1} = -\frac{\hbar e}{2V}\sum_{\mathbf{k},\nu\neq\xi}\frac{\mathrm{Im}[\langle\mathbf{s}\rangle_{\nu\xi}\langle\mathbf{v}\cdot\mathbf{E}\rangle_{\xi\nu}](\varepsilon_{\mathbf{k}\nu} - \varepsilon_{\mathbf{k}\xi})}{(\varepsilon_{\mathbf{k}\nu} - \varepsilon_{\mathbf{k}\xi})^2 + 4\Gamma^2} \times [\delta(\mu_F - \varepsilon_{\mathbf{k}\nu}) + \delta(\mu_F - \varepsilon_{\mathbf{k}\xi})], \tag{13}$$

$$\delta\mathbf{S}^{\mathrm{inter},2} = \frac{\hbar e}{V}\sum_{\mathbf{k},\nu\neq\xi}\frac{\mathrm{Re}[\langle\mathbf{s}\rangle_{\nu\xi}\langle\mathbf{v}\cdot\mathbf{E}\rangle_{\xi\nu}\Gamma]}{(\varepsilon_{\mathbf{k}\nu} - \varepsilon_{\mathbf{k}\xi})^2 + 4\Gamma^2} \times [\delta(\mu_F - \varepsilon_{\mathbf{k}\nu}) + \delta(\mu_F - \varepsilon_{\mathbf{k}\xi})]. \tag{14}$$

From here, one can see that the intraband contribution $\delta\mathbf{S}^{\mathrm{intra}}$ proportional to $1/\Gamma$ completely originates from the extrinsic perturbation. On the contrary, the interband contribution not only contributes to the extrinsic component $\delta\mathbf{S}^{\mathrm{inter},2}$, which is proportional to Γ, but also the intrinsic component $\delta\mathbf{S}^{\mathrm{inter},1}$, independent to the impurity scattering. With Eqs. (12)–(14), we in the following discuss the spin polarization and SOT for different scenarios.

III. RESULTS AND DISCUSSION FOR SOT

A. SOT without warping effect

First, we consider a simple scenario without warping effect $\lambda = 0$ and set an electric field along the x axis, $\mathbf{E} = E\hat{x}$. The off-diagonal elements are

$$\langle\boldsymbol{\sigma}\rangle_{+-} = \frac{Jm_z(J\mathbf{m}_\parallel + \hbar v_F\mathbf{k}\times\hat{z}) - \left(\varepsilon_{\mathbf{k}}^2 - J^2m_z^2\right)\hat{z}}{\varepsilon_{\mathbf{k}}\sqrt{\varepsilon_{\mathbf{k}}^2 - J^2m_z^2}} - i\frac{\hbar v_F\mathbf{k} + J\mathbf{m}_\parallel\times\hat{z}}{\sqrt{\varepsilon_{\mathbf{k}}^2 - J^2m_z^2}}, \tag{15}$$

and $\langle\boldsymbol{\sigma}\rangle_{-+} = [\langle\boldsymbol{\sigma}\rangle_{+-}]^\dagger$. The velocity operator is $\mathbf{v} = \frac{1}{\hbar}\nabla_{\mathbf{k}}H_{\mathrm{TI}} = v_F(\hat{z}\times\boldsymbol{\sigma})$. With these expressions, we find

$$\delta\mathbf{S}^{\mathrm{intra}} = -\frac{\hbar^2 v_F eE}{16\pi^2\Gamma\mu_F^2}\int d^2k(J\mathbf{m} + \hbar v_F\mathbf{k}\times\hat{z}) \times (Jm_y - \hbar v_F k_x)\delta(\mu_F - \varepsilon_{\mathbf{k}}), \tag{16}$$

$$\begin{aligned}\delta\mathbf{S}^{\mathrm{inter},1} = {} & \frac{\hbar^2 v_F eE}{16\pi^2}\frac{\mu_F}{\mu_F^2+\Gamma^2}\int d^2k\frac{Jm_x + hv_Fk_y}{\mu_F\left(\mu_F^2 - J^2m_z^2\right)} \\ & \times\left[Jm_z(J\mathbf{m} + \hbar v_F\mathbf{k}\times\hat{z}) - \mu_F^2\hat{z}\right]\delta(\mu_F - \varepsilon_{\mathbf{k}}) \\ & + \frac{\hbar^2 v_F eE}{16\pi^2}\frac{\mu_F}{\mu_F^2+\Gamma^2}\int d^2k\frac{Jm_z(Jm_y - hv_Fk_x)}{\mu_F\left(\mu_F^2 - J^2m_z^2\right)} \\ & \times(J\mathbf{m}\times\hat{z} - \hbar v_F\mathbf{k})\delta(\mu_F - \varepsilon_{\mathbf{k}}),\end{aligned} \tag{17}$$

$$\begin{aligned}\delta\mathbf{S}^{\mathrm{inter},2} = {} & \frac{\hbar^2 v_F eE}{16\pi^2}\frac{\Gamma}{\mu_F^2+\Gamma^2}\int d^2k\frac{Jm_z(Jm_y - hv_Fk_x)}{\mu_F\left(\mu_F^2 - J^2m_z^2\right)} \\ & \times\left[Jm_z(J\mathbf{m} + \hbar v_F\mathbf{k}\times\hat{z}) - \mu_F^2\hat{z}\right]\delta(\mu_F - \varepsilon_{\mathbf{k}}) \\ & - \frac{\hbar^2 v_F eE}{16\pi^2}\frac{\Gamma}{\mu_F^2+\Gamma^2}\int d^2k\frac{Jm_x + hv_Fk_y}{\mu_F\left(\mu_F^2 - J^2m_z^2\right)} \\ & \times(J\mathbf{m}\times\hat{z} - \hbar v_F\mathbf{k})\delta(\mu_F - \varepsilon_{\mathbf{k}}),\end{aligned} \tag{18}$$

where $\delta(\varepsilon_{\mathbf{k}} - \mu_F) = \frac{\mu_F}{\hbar v_F\sqrt{\mu_F^2 - J^2m_z^2}}\delta(k - k_F)$ with k_F the Fermi wave vector. Taking $\hbar v_F k_x - Jm_y \to \hbar v_F k_x'$ and $\hbar v_F k_y + Jm_x \to \hbar v_F k_y'$ and performing the integration of momentum, we have

$$\delta\mathbf{S}^{\mathrm{intra}} = -\frac{1 - \mathcal{J}^2m_z^2}{16\pi v_F}\frac{\mu_F}{\Gamma}(\hat{z}\times e\mathbf{E}), \tag{19}$$

$$\delta\mathbf{S}^{\mathrm{inter}} = \frac{\mathcal{J}}{8\pi v_F}m_z e\mathbf{E} - \frac{1 + \mathcal{J}^2m_z^2}{16\pi v_F}\frac{\Gamma}{\mu_F}(\hat{z}\times e\mathbf{E}), \tag{20}$$

with $\mathcal{J} = J/\mu_F$. Obviously, $\delta\mathbf{S} = \delta\mathbf{S}^{\mathrm{intra}} + \delta\mathbf{S}^{\mathrm{inter}}$ is in plane, either parallel ($\sim e\mathbf{E}$) or perpendicular ($\sim\hat{z}\times e\mathbf{E}$) to the current direction, while the z component of $\delta\mathbf{S}$ is strictly forbidden. Notice that only the out-of-plane magnetization m_z affects $\delta\mathbf{S}$ while the in-plane magnetization $m_{x/y}$ plays no role. Similar results are also reported in previous works [37,53]. Compared with those results, we further obtain an extra fieldlike term $\frac{1+\mathcal{J}^2m_z^2}{16\pi\hbar v_F}\frac{\Gamma}{\mu_F}(\hat{z}\times e\mathbf{E})$, which is proportional to Γ, originating from the extrinsic interband contribution. Besides, the intrinsic interband contribution, the first term in $\delta\mathbf{S}^{\mathrm{inter}}$, originating from the Berry curvature [34,53], vanishes if $m_z = 0$. The spin polarization of Dirac electrons causes the corresponding SOT, given by

$$\tau = \frac{2J}{\hbar}\mathbf{m}\times\delta\mathbf{S} = \tau_f\mathbf{m}\times(\hat{z}\times e\mathbf{E}) + \tau_d m_z e\mathbf{E}, \tag{21}$$

where $\tau_f = -\frac{\mathcal{J}(1-\mathcal{J}^2m_z^2)}{8\pi\hbar v_F}\frac{\mu_F^2}{\Gamma} - \frac{\mathcal{J}(1+\mathcal{J}^2m_z^2)}{8\pi\hbar v_F}\Gamma$ and $\tau_d = \frac{\mathcal{J}^2\mu_F}{4\pi\hbar v_F}$ are the strength of the fieldlike and antidampinglike SOTs, respectively. The former arises from the extrinsic inverse spin galvanic effect and the latter is from the intrinsic one.

B. SOT with warping effect

1. Hexagonal warping effect on spin polarization

In this section, we focus on the current-induced spin polarization $\delta\mathbf{S}$ by consideration of the hexagonal warping of TIs. Due to the warping term $\propto\sigma_z$, $\langle\sigma\rangle_{+-}$ and $\langle\boldsymbol{\sigma}\rangle_{-+}$ have similar forms as Eqs. (15) but $\varepsilon_{\mathbf{k}}$ include the contribution from warping effect λ, and Jm_z is replaced by $\Delta_{\mathbf{k}}$. The velocity operator is

$$\mathbf{v} = v_F(\hat{z}\times\boldsymbol{\sigma}) + \frac{3\lambda k^2}{\hbar}\sigma_z[\cos{(2\phi_k)}\hat{x} - \sin{(2\phi_k)}\hat{y}]. \tag{22}$$

With this formula, we can perform the same calculation procedure as before. The result can be written as $\delta\mathbf{S} = \delta\mathbf{S}^{\mathrm{in}} + \delta\mathbf{S}^{\mathrm{ex}}$ where $\delta\mathbf{S}^{\mathrm{in}}$ and $\delta\mathbf{S}^{\mathrm{ex}}$ are the intrinsic (scattering-independent) and the extrinsic (scattering-independent) spin polarization, respectively,

$$\delta\mathbf{S}^{\mathrm{in}} = -\frac{\mu_F e\hbar^2E}{4\left(\mu_F^2+\Gamma^2\right)}\int\frac{d^2k}{(2\pi)^2} \times \mathrm{Im}[\langle\boldsymbol{\sigma}\rangle_{+-}\langle v_x\rangle_{-+}]\delta(\mu_F - \varepsilon_{\mathbf{k}}), \tag{23}$$

$$\begin{aligned}\delta\mathbf{S}^{\mathrm{ex}} = {} & \frac{e\hbar^2E}{4\Gamma}\int\frac{d^2k}{(2\pi)^2}\langle\boldsymbol{\sigma}\rangle_{++}\langle v_x\rangle_{++}\delta(\mu_F - \varepsilon_{\mathbf{k}}) \\ & + \frac{\Gamma e\hbar^2E}{4\left(\mu_F^2+\Gamma^2\right)}\int\frac{d^2k}{(2\pi)^2} \\ & \times\mathrm{Re}[\langle\boldsymbol{\sigma}\rangle_{+-}\langle v_x\rangle_{-+}]\delta(\mu_F - \varepsilon_{\mathbf{k}}).\end{aligned} \tag{24}$$

Before demonstrating the numerical results of $\delta\mathbf{S}$ in FM/TI heterostructure with hexagonal warping, we derive their analytical expressions in the case of limit. Notice that the momentum shift $\hbar v_F k_x - Jm_y \to \hbar v_F k_x$ and $\hbar v_F k_y + Jm_x \to \hbar v_F k_y$ employed as before cannot eliminate the in-plane magnetization due to the snowflakelike Fermi surface. When using the relation $\delta(\mu_F - \varepsilon_{\mathbf{k}}) = \delta(k - k_F)/|\partial_k\varepsilon_{\mathbf{k}}|_{k=k_F}$, one has to find k_F satisfying $\varepsilon_{k_F} = \mu_F$. In the weak warping limit $\Lambda \ll \mathcal{J} < 1$ with $\Lambda = \lambda\mu_F^2/\hbar^3v_F^3$ and weak impurity scattering limit $\Gamma \to 0$, we keep Λ to the second order (detailed calculations see Sec. A in the Supplemental Material [58]) and obtain the approximate results as

$$\delta\mathbf{S}^{\mathrm{in}} = I_0\mathcal{J}\left(m_z\hat{\mathbf{E}} - 3\Lambda\tilde{\mathbf{m}}_\parallel + \tfrac{9}{2}\Lambda^2m_x\hat{z}\right), \tag{25}$$

$$\begin{aligned}\delta\mathbf{S}^{\mathrm{ex}} = {} & -\left[(I_{-1}+I_1) - (I_{-1}-I_1)\mathcal{J}^2m_z^2\right](\hat{z}\times\hat{\mathbf{E}}) \\ & + \tfrac{1}{2}\left[(I_{-1}+5I_1) + 9(I_{-1}+3I_1)\mathcal{J}^2\left(m_\parallel^2 - m_z^2\right)\right] \\ & \times\Lambda^2(\hat{z}\times\hat{\mathbf{E}}) - 3(I_{-1}+I_1)\Lambda\mathcal{J}^2(\mathbf{m}\times\tilde{\mathbf{m}}_\parallel)_z\hat{z} \\ & - 9(I_{-1}+3I_1)\Lambda^2\mathcal{J}^2(\mathbf{m}\times\tilde{\mathbf{m}}_\parallel)_y\hat{z}.\end{aligned} \tag{26}$$

Here, we denote $I_{-1} = \mu_F eE/(16\pi v_F \Gamma)$, $I_0 = eE/(8\pi v_F)$, and $I_1 = \Gamma eE/(16\pi v_F \mu_F)$, where the subscripts $(-1, 0, 1)$ in I represent the power of Γ. $\hat{\mathbf{E}}$ is the unit vector of $\mathbf{E}$ direction and $\tilde{\mathbf{m}}_\parallel = (m_y, m_x, 0)$ is a mirror vector of $\mathbf{m}_\parallel = (m_x, m_y, 0)$ with respect to $m_x = m_y$.

As λ (or Λ) vanishes, the current-induced spin polarization is reduced to $\delta\mathbf{S} = I_0 \mathcal{J} m_z \hat{\mathbf{E}} - [(I_{-1} + I_1) - (I_{-1} - I_1)\mathcal{J}^2 m_z^2](\hat{z} \times \hat{\mathbf{E}})$, where only m_z appears, recovering the results in Refs. [36,37] if ignoring the vertex correction. When a finite λ is introduced, the situation is greatly different from that for $\lambda = 0$, exhibiting complicated dependence on the orientation of $\mathbf{m}$. There appear extra contributions from the in-plane magnetizations m_x and m_y not grasped theoretically before, which is the focus of our study. From Eqs. (25) and (26), one can see several interesting results: (I) Even though $m_z = 0$, there still is nonzero spin polarization, which is contributed by the joint effect of the warping effect and the in-plane magnetization. The warping effect labeled with λ not only modifies the intrinsic component $\delta\mathbf{S}^{\text{in}}$ (characterized by I_0) but also the extrinsic component $\delta\mathbf{S}^{\text{ex}}$ (characterized by I_{-1} and I_1). The former is realized through modifying the Berry curvature of energy bands, which can be understood from Eq. (4), where the Berry curvature is modified by the finite warping together with the in-plane magnetization. (II) The modified intrinsic part makes the dampinglike term $\delta\mathbf{S}^{\text{in}}$, which is odd upon magnetization $\mathbf{m}$ reversal, deviate from usual current direction $\hat{\mathbf{E}}$, and the modified extrinsic part makes the fieldlike term $\delta\mathbf{S}^{\text{ex}}$, which is even upon magnetization $\mathbf{m}$ reversal, deviate from $\hat{z} \times e\mathbf{E}$. (III) More importantly, there comes up an out-of-plane part $\sim\hat{z}$ in both $\delta\mathbf{S}^{\text{in}}$ and $\delta\mathbf{S}^{\text{ex}}$. Note that the out-of-plane component δS_z remains zero if $\mathbf{m}$ is perpendicular to the surface even for a finite λ. It is well known that for the FM/TI bilayer without warping term, the orientation of the spin polarization in the weak exchange limit is along the TI surface, controlled by the spin momentum locking. As a consequence, the total spin polarization $\delta\mathbf{S} = \delta\mathbf{S}^{\text{in}} + \delta\mathbf{S}^{\text{ex}}$ is not only dependent on m_z but on $m_{x/y}$ and the resulting SOT shows sensitive to the azimuthal angle of the FM magnetization.

Above, we present the analysis about the role of in-plane FM magnetization and the warping effect of TIs. To obtain accurate results, we carry out the numerical calculations on $\delta\mathbf{S}$ directly starting from formula Eqs. (23) and (24). In Fig. 2, we demonstrate the dependence of $\delta\mathbf{S}$ on the FM magnetization direction, where the polar angle θ_m and the azimuthal angle ϕ_m are defined in Fig. 1(a). In Figs. 2(a)–2(c), we arrange the FM magnetization in plane (i.e., keeping polar angle $\theta_m = \pi/2$) and tune the azimuthal angle ϕ_m. For $\lambda = 0$, naturally, all components of $\delta\mathbf{S}$ are independent on the azimuthal angle ϕ_m due to $m_{x/y}$ having no contribution, in agreement with previous theoretical results [37]. Finite δS_x and δS_z appear and oscillate with enhanced amplitude as λ increases. The former exhibits 2π-period oscillation due to the contribution from $\tilde{\mathbf{m}}_\parallel = (m_y, m_x, 0)$ while the latter is π-period oscillation due to different symmetry along the z axis and x axis. In fact, δS_z exhibits a complex oscillation type owing to the competition between a threefold function of momentum in Hamiltonian and a twofold function of momentum in velocity operator Eq. (22), as shown in the inset of Fig. 2(c) which presents different oscillation behaviors for different polar angles θ_m. Only when $\theta_m = \pi/2$, the oscillation is reduced to be $\cos 2\phi_m$. On the contrary, δS_y, proportional to $(\hat{z} \times \hat{\mathbf{E}})$, is independent on ϕ_m though it is also sensitive to the size of λ. These results are obvious since δS_y in Eq. (26) is affected only by the size of the in-plane magnetization $(\mathbf{m}_\parallel^2)$ corrected by a factor Λ^2. These interesting results stem from the joint effect of warping effect and in-plane magnetization, and without either one ϕ_m dependence will disappear. As we know, this dependence is not reported theoretically before, which provides a new perspective to understand the related experiments [22,27] where the in-plane magnetic field was adopted.

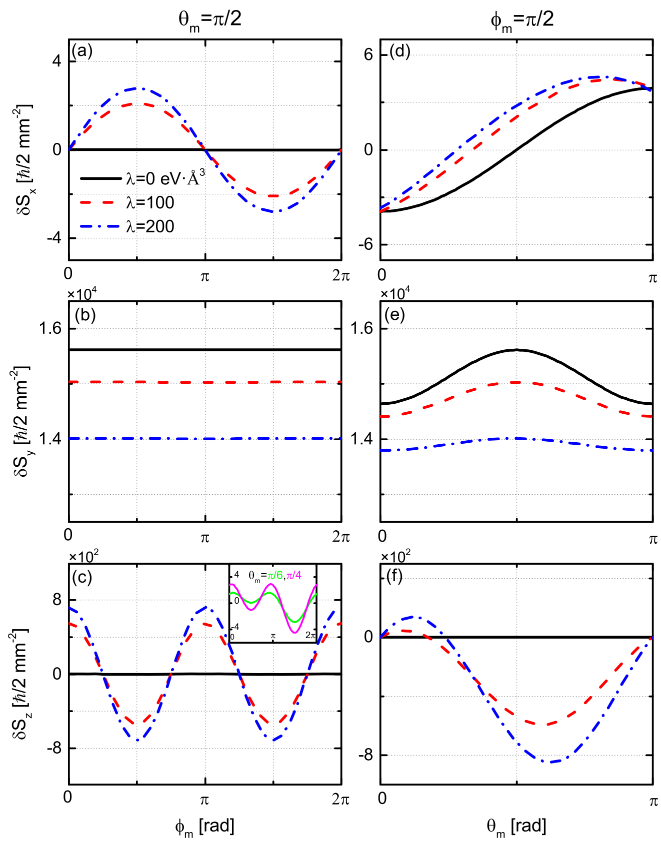

FIG. 2. (a)–(c) Azimuthal angle ϕ_m dependence of the current-induced spin polarization $\delta\mathbf{S}$ with fixed $\theta_m = \pi/2$ and (d)–(f) dependence of $\delta\mathbf{S}$ on θ_m with fixed $\phi_m = \pi/2$, for different warping parameters λ. We set $\mu_F = 0.2$ eV, $J = 0.05$ eV, and $\Gamma = 0.1$ meV.

In Figs. 2(d)–2(f), we display the dependence of $\delta\mathbf{S}$ on the polar angle θ_m of $\mathbf{m}$ with fixed azimuthal angle $\phi_m = \pi/2$. Without the warping effect ($\lambda = 0$), δS_x is strictly antisymmetric with respect to $\theta_m = \pi/2$, indicating the behavior $\delta S_x \propto m_z$, but δS_y is strictly symmetric. As finite λ is turned on, the antisymmetry of δS_x is broken due to curves shifting upwards while δS_z develops an oscillation. Obviously, these behaviors are caused by the extra contribution from the in-plane magnetization m_x and m_y. If the magnetization $\mathbf{m}$ is arranged strictly along the z axis $\mathbf{m} = (0, 0, 1)$, seeing $\theta_m = 0$ or π, δS_x and δS_z are regardless of the strength of λ because of no available in-plane magnetization. In contrast, δS_y is dependent on λ stemming from $m_z^2(\hat{z} \times \hat{\mathbf{E}})$ in Eq. (26). It is emphasized that nonzero out-of-plane component δS_z

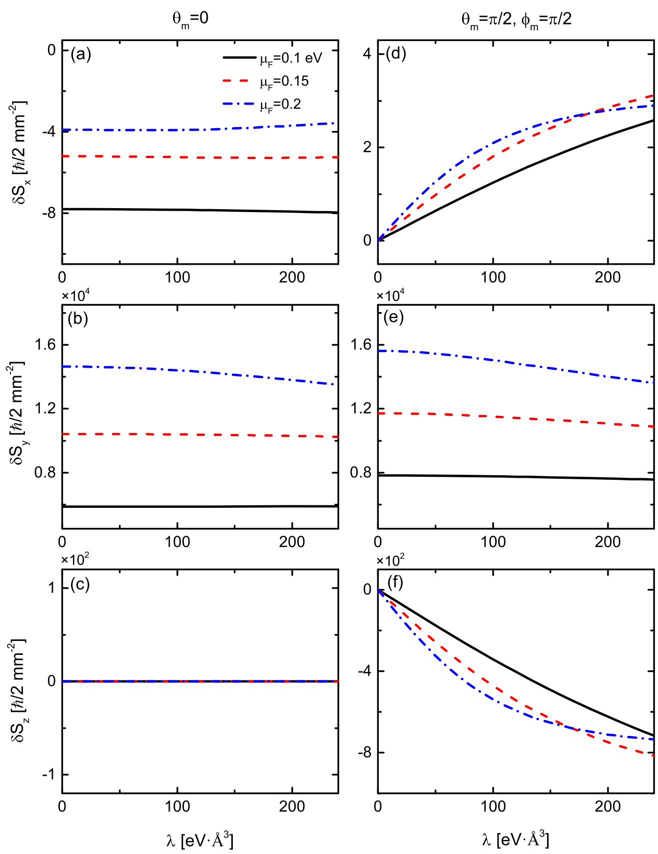

FIG. 3. Variation of the current-induced spin polarization $\delta\mathbf{S}$ with the warping parameter λ for different Fermi energies μ_F under (a)–(c) $\mathbf{m} \parallel \hat{z}(\theta_m = 0)$ and (d)–(f) $\mathbf{m} \perp \hat{z}(\theta_m = \pi/2)$.

and its significant dependence on the orientation of $\mathbf{m}$ in Figs. 2(c) and 2(f) originate from the joint effect of the warping effect and the in-plane magnetization. Without the warping effect or the in-plane magnetization, δS_z will always vanish.

Since the snowflakelike Fermi surface induced by warping effect is sensitive to the Fermi energy μ_F, we in Fig. 3 depict the variation of δS_x, δS_y, and δS_z with warping parameter λ for different values of μ_F. To compare, we plot two limited cases: $\mathbf{m}$ perpendicular to the surface ($\theta_m = 0$) in Figs. 3(a)–3(c) and along the TI surface ($\theta_m = \pi/2$) in Figs. 3(d)–3(f). When the magnetization is chosen perpendicular to the plane ($\theta_m = 0$) and no in-plane components, all components of $\delta\mathbf{S}$ are quite insensitive to the warping parameter λ even for large μ_F. Especially, no finite δS_z appears no matter what the value of the warping parameter λ and μ_F. These numerical results are in agreement with our analytic formula in Eqs. (25) and (26). The slight variation with λ stems from the high order terms of Λ, not including in Eqs. (25) and (26). Therefore, for $\mathbf{m}$ perpendicular to the surface, the effect of warping effect on the current-induced spin polarization can be ignored even for high μ_F. On the contrary, the scenario is heavily different when the magnetization is orientated to be in-plane ($\theta_m = \pi/2$), shown in Figs. 3(d)–3(f). All components of $\delta\mathbf{S}$ are sensitive to warping parameter λ, especially for δS_x and δS_z. The magnitudes of δS_x and δS_z increase with λ in a linearlike behavior for low Fermi level μ_F. When μ_F is lifted, the lineshape on parameter λ deviates from the linearlike behavior. Unlike this, the component δS_y shows weaker decay with λ for large μ_F. These results are associated with the decreased density of states [48] and change of the Berry curvature with a nonzero λ for large chemical potential.

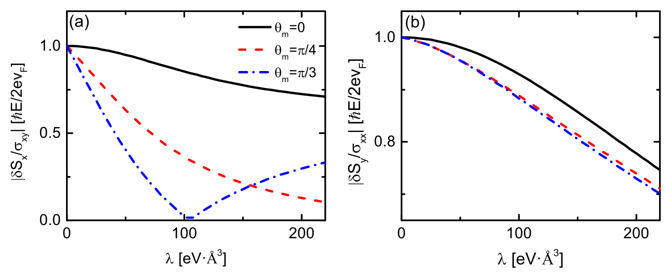

FIG. 4. Ratios (a) $|\delta S_x/\sigma_{xy}|$ and (b) $|\delta S_y/\sigma_{xx}|$ as a function of the warping parameter λ for different polar angles θ_m.

2. The relation between spin polarization and conductivity

Spin-momentum locking in linear dispersion draws an equivalence between the electric current $\mathbf{j}$ on the surface of magnetic TIs and the in-plane components of the spin polarization $\delta\mathbf{S}$. In the zero λ case, the helical surface states ensure the identity between charge current $\mathbf{j}$ and electron spin σ by the relation $\mathbf{j} = ev_F(\hat{z} \times \boldsymbol{\sigma})$. However, this identity is distinctly broken while λ is turned on. One can recall that the electric field driven dc conductivity in the FM/TI interface can be calculated in a similar procedure within the linear response theory:

$$\sigma_{\alpha x} = -\lim_{\Omega\to 0}\frac{1}{\Omega E}\mathrm{Im}\Pi^R_{j_\alpha, j_x}(\Omega + i0^+), \tag{27}$$

where $\alpha = x, y$ and the symbol $\sigma_{xx}(\sigma_{xy})$ is longitudinal (Hall) conductivity. Without λ, the ratio of spin polarization and conductivity is a constant [33,36]:

$$\delta S_x = \frac{\hbar E}{2ev_F}\sigma_{xy}, \quad \delta S_y = -\frac{\hbar E}{2ev_F}\sigma_{xx}, \tag{28}$$

which implies the spin polarization can be detected through measuring the conductivity. In the case with hexagonal warping effect, however, ratio $|\delta S_\alpha/\sigma_{x\gamma}|$ is not still a constant but depends on the systemic parameters. Figure 4 illustrates the variation of ratio $|\delta S_\alpha/\sigma_{x\gamma}|$ with λ for different magnetization orientation. Obviously, with the increase of λ the ratios $|\delta S_x/\sigma_{xy}|$ and $|\delta S_y/\sigma_{xx}|$ heavily deviate from the constant $\hbar E/2ev_F$, and the deviated extent is dependent on the magnetization orientation, e.g., θ_m. When $|\delta S_y/\sigma_{xx}|$ decays monotonously with λ, $|\delta S_x/\sigma_{xy}|$ exhibits prominent nonmonotonic change and even vanishes at certain values of λ, which stems from the strong dependence on the in-plane magnetization m_x and m_y. Only when $\mathbf{m}$ is perpendicular to the surface ($\theta_m = 0$), the ratios can almost remain a constant for smaller λ.

3. Hexagonal warping effect on SOT

When an applied current generates the nonequilibrium spin polarization $\delta\mathbf{S}$ on the TI surface, the adjacent FM

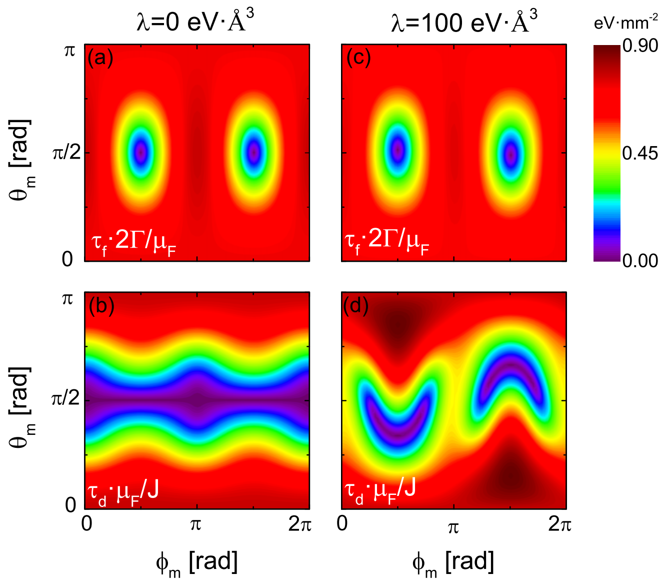

FIG. 5. Magnitude of the fieldlike SOT τ_f and dampinglike SOT τ_d as functions of the magnetization direction $[(\theta_m, \phi_m)]$. The left panels (a) and (b) for $\lambda = 0$ and the right panels (c) and (d) for $\lambda = 100\,\text{eV}\,\text{Å}^3$. The other parameters are the same as Fig. 1 and Fig. 2.

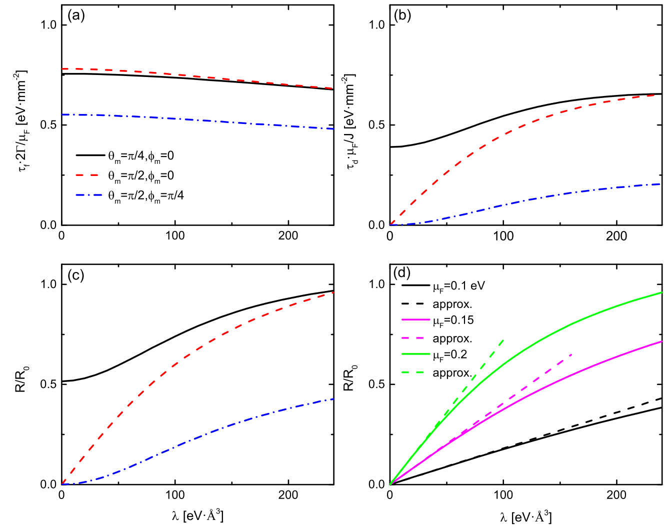

FIG. 6. (a)–(c) Magnitude of FL-SOT τ_f and DL-SOT τ_d and their ratio $R = \tau_d/\tau_f$, respectively, as a function of warping parameter λ for different polar angles θ_m. (d) Comparison between numerical and approximate results of the ratio for different Fermi energies μ_F.

layer feels a SOT as $\tau = \frac{2J}{\hbar}\mathbf{m} \times \delta\mathbf{S}$. The torque is generally decomposed into two parts according to its symmetry and antisymmetry with respect to the magnetization reversal ($\mathbf{m} \to -\mathbf{m}$), namely, the FL-SOT τ_{FL} and the DL-SOT τ_{DL}. One can straightforwardly check that $\mathbf{m} \times \delta\mathbf{S}^{\text{ex}}$ is asymmetric and $\mathbf{m} \times \delta\mathbf{S}^{\text{in}}$ is symmetric, and so the FL and DL torques are

$$\tau_{\text{FL}} = \frac{2J}{\hbar}\mathbf{m} \times \delta\mathbf{S}^{\text{ex}},$$
$$\tau_{\text{DL}} = \frac{2J}{\hbar}\mathbf{m} \times \delta\mathbf{S}^{\text{in}}. \tag{29}$$

From Eqs. (25) and (26) we can see that the total torque cannot be expressed in the form of $\tau = \tau_f \mathbf{m} \times (\hat{z} \times e\mathbf{E}) + \tau_d m_z \mathbf{m} \times e\mathbf{E}$ as in the TIs without hexagonal warping or more generally form in 2D electron gas $\tau = \tau_f \mathbf{m} \times (\hat{z} \times e\mathbf{E}) + \tau_d \mathbf{m} \times [(\hat{z} \times e\mathbf{E}) \times \mathbf{m}]$. The warping effect introduces a more complicated dependence on the magnetization direction associated with the distortion of the band structure as in Fig. 1. Even so, we still can determine the magnitude of the FL-SOT $\tau_f = |\tau_{\text{FL}}|$ and the DL-SOT $\tau_d = |\tau_{\text{DL}}|$ according to their odd and even function with respect to $\mathbf{m}$. With Eqs. (23) and (24) we numerically calculate τ_f and τ_d and present the corresponding results in Fig. 5 as functions of the $\mathbf{m}$ direction (θ_m, ϕ_m). We plot SOT in Figs. 5(a) and 5(b) for $\lambda = 0$ and in Figs. 5(c) and 5(d) for finite λ. For $\lambda = 0$, the FL-SOT term τ_f in Fig. 5(a) shows insensitive to the direction angle (θ_m, ϕ_m) except for around $\theta_m = \phi_m = k\pi/2$, where the torque vanishes due to $\mathbf{m} \parallel \delta\mathbf{S}^{\text{ex}}$. The finite λ only slightly affects τ_f [seeing Fig. 5(c)] since the dominant component δS_y^{ex} is insensitive to the warping parameter λ, as illustrated in Figs. 3(b)–3(e). In contrast, the DL-SOT term τ_d for $\lambda = 0$ in Fig. 5(b) shows the oscillating dependence, determined by the factor $m_z|\mathbf{m}\times\hat{x}|$. When finite λ is induced further, the oscillating behaviors of τ_d with θ_m and ϕ_m are significantly changed in Fig. 5(d). This originates from the λ-induced other components of $\delta\mathbf{S}^{\text{in}}$ along the y and z axis. This prominent variation implies that one can crease the DL-SOT term by tuning the parameter λ. In order to clarify the behavior of λ, we plot the FL-SOT τ_f in Fig. 6(a), DL-SOT τ_d in Fig. 6(b), and their ratio $R = \tau_d/\tau_f$ in Fig. 6(c) as a function of warping parameter λ. While τ_f is insensitive to the parameter λ, τ_d is significantly enhanced by λ, especially for the magnetization oriented along the TI surface (i.e., $\theta_m = \pi/2$). As a consequence, the ratio R is increased significantly by λ with the magnitude depending on the $\mathbf{m}$ direction (θ_m, ϕ_m), as shown in Fig. 6(c). Importantly, in the presence only of an in-plane magnetization ($\theta_m = \pi/2$), the DL-SOT is contributed completely by the warping effect. In this situation, the ratio for small warping parameter λ (or Λ) can be approximated as

$$R \approx R_0 \frac{3\Lambda}{\sqrt{1 + 9\Lambda^2\mathcal{J}^4\left(m_x^2 - m_y^2\right)^2}}, \tag{30}$$

with $R_0 = 2\Gamma\mathcal{J}/\mu_F$. The approximate values are compared with the numerical results in Fig. 6(d). The enhancement of DL-SOT τ_d by the joint effect of the hexagonal warping and the in-plane magnetization provides a new perspective to understand the giant antidampinglike SOT observed experimentally.

IV. DISCUSSION

In this section, we want to remark the effect of vertex corrections. The impurity-renormalized velocity in general takes the form

$$V_x = v_x + \delta V_x = v_x + n_i u_0^2 \int \frac{d^2k}{(2\pi)^2} G_{\mathbf{k}}^R V_x G_{\mathbf{k}}^A. \tag{31}$$

By setting $\delta V_x = A\sigma_0 + B\sigma_x + C\sigma_y + D(k_x^2 - k_y^2)\sigma_z$, we can solve all the coefficients, seeing the detailed derivation in

Sec. B of the Supplemental Material [58]. In the absence of the warping term and $\mathcal{J} \ll 1$, we find $V_x = 2v_x$. In the presence of the warping term, the vertex correction gives $A = D = 0$. The nonzero C is to renormalize the Fermi velocity v_F in Eq. (22) to be $v_{Fy} = v_F(1 + C)$, while $B\sigma_x$ leads to a new velocity component. The calculated spin polarization $\delta\mathbf{S}$ by taking into account the vertex corrections is given in Eqs. (B19) and (B20) in the Supplemental Material [58]. Compared with Eqs. (25) and (26), it is obvious to find that the vertex correction has two effects: (1) modifies the constant factors before I_n in $\delta\mathbf{S}^{\rm in}$ and $\delta\mathbf{S}^{\rm ex}$. Especially, the corrected different factors before m_x^2 and m_y^2 in $\delta\mathbf{S}^{\rm ex}$ make δS_y shown in Fig. 2(b) weakly dependent on magnetic azimuthal angle ϕ_m; (2) brings an extra term $\Delta = -\Lambda(I_{-1} + 13I_1)\mathcal{J}^2 m_x m_z \hat{x} + 3\Lambda^2(I_{-1} + I_1)\mathcal{J}^2 m_x m_y \hat{x} + 2\Lambda(I_{-1} + I_1)\mathcal{J}^2 m_y m_z \hat{y}$ to $\delta\mathbf{S}^{\rm ex}$. The term $\sim m_y m_z$ along the y direction makes δS_y extra depend on the in-plane angle ϕ_m, which modulates the curves of δS_y in Fig. 2(e) slightly asymmetric to $\theta_m = \pi/2$. The other two new terms affect the dependence of spin polarization δS_x on magnetic azimuthal angle ϕ_m. For example, the term $\sim m_x m_y$ makes the oscillating period of δS_x shown in Fig. 2(a) change from 2π to π. For the in-plane field $\theta_m = \pi/2$ which is our focus, only the term $\sim m_x m_y$ plays a role. It is noticed that the extra term Δ induced by the vertex corrections only corrects the $\delta\mathbf{S}^{\rm ex}$, which does not affect the behavior of the dampinglike spin torque.

In the self-energy of the Green's function in Eq. (8), we only take into account the spin-independent component $i\Gamma$ for convenience to derive the analytical expressions. When the hexagonal warping and magnetization are considered, additional spin-dependent terms in self-energy appear, seeing the detailed derivation in Sec. C of the Supplemental Material [58]. For weak warping under consideration, to second order in the warping parameter Λ, we obtain the imaginary part of the self-energy as $\mathrm{Im}\,\Sigma^R = -i\Gamma\sum_{a=0,x,y,z} w_a\sigma_a$ with $w_0 = (1 - \frac{3}{2}\Lambda^2)$, $w_x = -3\mathcal{J}m_x\Lambda^2$, $w_y = -\frac{7}{2}\mathcal{J}m_y\Lambda^2$, and $w_z = \mathcal{J}m_z(1 - \Lambda^2)$. Since we focus on the regime of $\Lambda \ll \mathcal{J} < 1$, the spin-dependent components w_x and w_y and the second terms in w_0 and w_z, as higher-order terms of warping parameter, can be ignored. The diagonal component w_z only provides a self-energy $\Gamma\mathcal{J}m_z\sigma_z$ to weakly correct the constant factors in the first term of Eq. (26). Since our study focuses on the combination effect of the in-plane magnetization and the warping effect, for weak impurity scattering, ignoring the spin-dependence components in the self-energy would not affect our main results.

In our study, we start from the effective Hamiltonian in Eq. (1), where the magnetic exchange interaction $J\mathbf{m}\cdot\boldsymbol{\sigma}$ between conducting electrons and the FM layer is added due to magnetic proximity effect. When the FM layer is metallic, the TI surface states are strongly coupled with the FM metallic states. To grasp this physics, we can start from a more general FM-TI coupling Hamiltonian $H_{\rm full} = \begin{pmatrix} H_{\rm FM} & j_{\rm ex} \\ j_{\rm ex}^* & H_{\rm TI}\end{pmatrix}$, where $H_{\rm FM}$ is the Hamiltonian of the FM metal and $j_{\rm ex}$ is the FM-TI coupling strength. By performing the equation of motion with respect to $H_{\rm full}$ and tracing the degrees of freedom of the FM, we can obtain the TI-subsystem Green's function and then an effective Hamiltonian of the TI layer, $H_{\rm TI,eff} = H_{\rm TI} + j_{\rm ex}^*(\varepsilon - H_{\rm FM})^{-1} j_{\rm ex}$. Taking the FM metal in a typical form of $H_{\rm FM} = \alpha k^2 + \delta\mu + \Delta_{\rm FM}\mathbf{m}\cdot\boldsymbol{\sigma}$, with $\alpha = \hbar/2m_e$ the inverse mass, $\delta\mu$ the mismatch of Fermi surface between FM and TI bands, and $\Delta_{\rm FM}$ the exchange energy within the FM, the effective Hamiltonian reduces to $H_{\rm TI,eff} = H_{\rm TI} + \mu_0(\varepsilon) + J_0(\varepsilon)\mathbf{m}\cdot\boldsymbol{\sigma}$, where $\mu_0(\varepsilon) = |j_{\rm ex}|^2(\varepsilon - \varepsilon_0)/[(\varepsilon - \varepsilon_0)^2 - \Delta_{\rm FM}^2]$ and $J_0(\varepsilon) = |j_{\rm ex}|^2\Delta_{\rm FM}/[(\varepsilon - \varepsilon_0)^2 - \Delta_{\rm FM}^2]$ with $\varepsilon_0 = \alpha k^2 + \delta\mu$. Obviously, $\mu_0(\varepsilon)$ is to modify the dispersion of TI energy bands and $J_0(\varepsilon)$ is the effective exchange energy from the FM. When the energy-dispersion dependence of $\mu_0(\varepsilon)$ and $J_0(\varepsilon)$ can be ignored, for example, taking large mismatch energy $\delta\mu$, in which $\mu_0(\varepsilon) \approx -|J|^2\delta\mu/[(\delta\mu)^2 - \Delta_{\rm FM}^2]$ and $J_0(\varepsilon) \approx |J|^2\Delta_{\rm FM}/[(\delta\mu)^2 - \Delta_{\rm FM}^2]$, we reach Eq. (1). Therefore, the effective Hamiltonian in Eq. (1) is valid in the condition of the bottom of the FM band far away from the Dirac point or not very large Fermi level in TI. In our study, we keep a relative small Fermi energy and the main results, obtained analytically and numerically, are reliable. Experimentally, in order to ensure the large mismatch energy in the FM-TI heterostructure and minimize the current shutting effect through the FM layer, one can use the FM material with high resistivity as in Refs. [22,24,25,27].

In conclusion, current-induced spin polarization and resulting SOT in the FM/TI bilayer have been investigated. We find that the usually ignored in-plane FM magnetization plays an important role when hexagonal warping of topological surface states is taken into account. Not only the out-of-plane magnetization m_z but also the in-plane magnetizations m_x and m_y contribute to the spin-orbit torque. As a consequence, the resulting spin polarization and spin torque significantly depend on the FM magnetic direction, importantly exhibiting a remarkable dependence on the azimuthal angle of magnetization, which has not been reported theoretically before in the linear dispersion TI model. We also obtain the out-of-plane spin polarization δS_z component, which cannot yield in the linear TI model. These interesting results arise from the combination effect of in-plane magnetization and warping effect, which induces new intrinsic contribution and extrinsic contribution by modifying the Berry curvature and impurity scattering. We analyze the results analytically and numerically, starting from derivation of the formula of nonequilibrium spin polarization based on Matsubara-Green function approach. Besides, we discuss the nonlinear relation between the current-induced spin polarization and the dc conductivity. More importantly, it is found that the warping effect can significantly enhance the antidamping SOT if there exists the in-plane FM magnetization, which provides a new perspective to understand the recent giant SOT effect.

ACKNOWLEDGMENTS

This work was supported by GDUPS (2017), by National Natural Science Foundation of China (Grants No. 11874016, 11474106, and No. 11774100) and by Key Program for Guangdong NSF of China (Grant No. 2017B030311003).

[1] G. Prenat, K. Jabeur, G. D. Pendina, O. Boulle, G. Gaudin, W. Zhao, and G. Prenat, Beyond STT-MRAM spin orbit torque RAM SOT-MRAM for high speed and high reliability applications, in *Spintronics-Based Computing* (Springer, Switzerland, 2015), pp. 145–157.
[2] A. Manchon, I. M. Miron, T. Jungwirth, J. Sinova, J. Železný, A. Thiaville, K. Garello, and P. Gambardella, Current-induced spin-orbit torques in ferromagnetic and antiferromagnetic systems, arXiv:1801.09636.
[3] I. Garate and A. H. MacDonald, Influence of a transport current on magnetic anisotropy in gyrotropic ferromagnets, Phys. Rev. B **80**, 134403 (2009).
[4] J. Sinova, S. O. Valenzuela, J. Wunderlich, C. H. Back, and T. Jungwirth, Spin Hall effects, Rev. Mod. Phys. **87**, 1213 (2015).
[5] G. Prenat, K. Jabeur, P. Vanhauwaert, G. Di Pendina, F. Oboril, R. Bishnoi, M. Ebrahimi, N. Lamard, O. Boulle, K. Garello, J. Langer, B. Ocker, M. C. Cyrille, P. Gambardella, M. Tahoori, and G. Gaudin, Ultra-Fast and high-reliability SOT-MRAM: From cache Replacement to normally-off computing, IEEE Trans. Multi-Scale Computing Systems **2**, 49 (2016).
[6] I. M. Miron, G. Gaudin, S. Auffret, B. Rodmacq, A. Schuhl, S. Pizzini, J. Vogel, and P. Gambardella, Current-driven spin torque induced by the Rashba effect in a ferromagnetic metal layer, Nat. Mater. **9**, 230 (2010).
[7] I. M. Miron, K. Garello, G. Gaudin, P.-J. Zermatten, M. V. Costache, S. Auffret, S. Bandiera, B. Rodmacq, A. Schuhl, and P. Gambardella, Perpendicular switching of a single ferromagnetic layer induced by in-plane current injection, Nature (London) **476**, 189 (2011).
[8] J. Železný, H. Gao, K. Výborn ý, J. Zemen, J. Mašek, A. Manchon, J. Wunderlich, J. Sinova, and T. Jungwirth, Relativistic Néel-Order Fields Induced by Electrical Current in Antiferromagnets, Phys. Rev. Lett. **113**, 157201 (2014).
[9] J. Železný, H. Gao, A. Manchon, F. Freimuth, Y. Mokrousov, J. Zemen, J. Mašek, J. Sinova, and T. Jungwirth, Spin-orbit torques in locally and globally noncentrosymmetric crystals: Antiferromagnets and ferromagnets, Phys. Rev. B **95**, 014403 (2017).
[10] M. Trushin and J. Schliemann, Anisotropic current-induced spin accumulation in the two-dimensional electron gas with spin-orbit coupling, Phys. Rev. B **75**, 155323 (2007).
[11] U. H. Pi, K. W. Kim, J. Y. Bae, S. C. Lee, Y. J. Cho, K. S. Kim, and S. Seo, Tilting of the spin orientation induced by Rashba effect in ferromagnetic metal layer, Appl. Phys. Lett. **97**, 162507 (2010).
[12] I. M. Miron, T. Moore, H. Szambolics, L. D. Buda-Prejbeanu, S. Auffret, B. Rodmacq, S. Pizzini, J. Vogel, M. Bonfim, A. Schuhl, and G. Gaudin, Fast current-induced domain-wall motion controlled by the Rashba effect, Nat. Mater. **10**, 419 (2011).
[13] T. Suzuki, S. Fukami, N. Ishiwata, M. Yamanouchi, S. Ikeda, N. Kasai, and H. Ohno, Current-induced effective field in perpendicularly magnetized Ta/CoFeB/MgO wire, Appl. Phys. Lett. **98**, 142505 (2011).
[14] L. Liu, C.-F. Pai, D. C. Ralph, and R. A. Buhrman, Magnetic Oscillations Driven by the Spin Hall Effect in 3-Terminal Magnetic Tunnel Junction Devices, Phys. Rev. Lett. **109**, 186602 (2012).
[15] E. van der Bijl and R. A. Duine, Current-induced torques in textured Rashba ferromagnets, Phys. Rev. B **86**, 094406 (2012).
[16] P. M. Haney, H.-W. Lee, K.-J. Lee, A. Manchon, and M. D. Stiles, Current induced torques and interfacial spin-orbit coupling: Semiclassical modeling, Phys. Rev. B **87**, 174411 (2013).
[17] T. D. Skinner, K. Olejník, L. K. Cunningham, H. Kurebayashi, R. P. Campion, B. L. Gallagher, T. Jungwirth, and A. J. Ferguson, Complementary spin-Hall and inverse spin-galvanic effect torques in a ferromagnet/semiconductor bilayer, Nat. Commun. **6**, 6730 (2015).
[18] L. Chen, M. Gmitra, M. Vogel, R. Islinger, M. Kronseder, D. Schuh, D. Bougeard, J. Fabian, D. Weiss, and C. H. Back, Electric-field control of interfacial spin-orbit fields, Nat. Electron. **1**, 350 (2018).
[19] M. Z. Hasan and C. L. Kane, Topological insulators, Rev. Mod. Phys. **82**, 3045 (2010).
[20] X.-L. Qi and S.-C. Zhang, Topological insulators and superconductors, Rev. Mod. Phys. **83**, 1057 (2011).
[21] O. V. Yazyev, J. E. Moore, and S. G. Louie, Spin Polarization and Transport of Surface States in the Topological Insulators Bi_2Se_3 and Bi_2Te_3 from First Principles, Phys. Rev. Lett. **105**, 266806 (2010).
[22] Y. Wang, P. Deorani, K. Banerjee, N. Koirala, M. Brahlek, S. Oh, and H. Yang, Topological Surface States Originated Spin-Orbit Torques in Bi_2Se_3, Phys. Rev. Lett. **114**, 257202 (2015).
[23] C. H. Li, O. M. J. van't Erve, S. Rajput, L. Li, and B. T. Jonker, Direct comparison of current-induced spin polarization in topological insulator Bi_2Se_3 and InAs Rashba states, Nat. Commun. **7**, 13518 (2016).
[24] Y. Wang, D. Zhu, Y. Wu, Y. Yang, J. Yu, R. Ramaswamy, R. Mishra, S. Shi, M. Elyasi, K.-L. Teo, Y. Wu, and H. Yang, Room temperature magnetization switching in topological insulator-ferromagnet heterostructures by spin-orbit torques, Nat. Commun. **8**, 1364 (2017).
[25] M. DC, R. Grassi, J.-Y. Chen, M. Jamali, D. R. Hickey, D. Zhang, Z. Zhao, H. Li, P. Quarterman, Y. L. M. Li, A. Manchon, K. A. Mkhoyan, T. Low, and J.-P. Wang, Room-temperature high spin-orbit torque due to quantum confinement in sputtered Bi_xSe_{1-x} films, Nat. Mater. **17**, 800 (2018).
[26] A. R. Mellnik, J. S. Lee, A. Richardella, J. L. Grab, P. J. Mintun, M. H. Fischer, A. Vaezi, A. Manchon, E.-A. Kim, N. Samarth, and D. C. Ralph, Spin-transfer torque generated by a topological insulator, Nature (London) **511**, 449 (2014).
[27] Y. Fan, P. Upadhyaya, X. Kou, M. Lang, S. Takei, Z. Wang, J. Tang, L. He, L.-T. Chang, M. Montazeri, G. Yu, W. Jiang, T. Nie, R. N. Schwartz, Y. Tserkovnyak, and K. L. Wang, Magnetization switching through giant spin-orbit torque in a magnetically doped topological insulator heterostructure, Nat. Mater. **13**, 699 (2014).
[28] Y. Fan, X. Kou, P. Upadhyaya, Q. Shao, L. Pan, M. Lang, X. Che, J. Tang, M. Montazeri, K. Murata, L.-T. Chang, M. Akyol, G. Yu, T. Nie, K. L. Wong, J. Liu, Y. Wang, Y. Tserkovnyak, and K. L. Wang, Electric-field control of spin-orbit torque in a magnetically doped topological insulator, Nat. Nanotechnol. **11**, 352 (2016).
[29] J. Han, A. Richardella, S. A. Siddiqui, J. Finley, N. Samarth, and L. Liu, Room-Temperature Spin-Orbit Torque Switching Induced by a Topological Insulator, Phys. Rev. Lett. **119**, 077702 (2017).
[30] J. Sinova and T. Jungwirth, Surprises from the spin Hall effect, Phys. Today **70**(7), 38 (2017).

[31] V. M. Edelstein, Spin Polarization of conduction electrons induced by electric current in two-dimensional asymmetric electron systems, Solid State Commun. **73**, 233 (1990).
[32] V. V. Belkov and S. D. Ganichev, Magnetogyrotropic effects in semiconductor quantum wells, Semicond. Sci. Technol. **23**, 114003 (2008).
[33] I. Garate and M. Franz, Inverse Spin-Galvanic Effect in the Interface between a Topological Insulator and a Ferromagnet, Phys. Rev. Lett. **104**, 146802 (2010).
[34] H. Kurebayashi, J. Sinova, D. Fang, A. C. Irvine, T. D. Skinner, J. Wunderlich, V. Novák, R. P. Campion, B. L. Gallagher, E. K. Vehstedt, L. P. Zârbo, K. Výborný, A. J. Ferguson, and T. Jungwirth, An antidamping spin-orbit torque originating from the Berry curvature, Nat. Nanotechnol. **9**, 211 (2014).
[35] H. Li, H. Gao, L. P. Zârbo, K. Výborný, X. Wang, I. Garate, F. Doğan, A. Čejchan, J. Sinova, T. Jungwirth, and A. Manchon, Intraband and interband spin-orbit torques in noncentrosymmetric ferromagnets, Phys. Rev. B **91**, 134402 (2015).
[36] A. Sakai and H. Kohno, Spin torques and charge transport on the surface of topological insulator, Phys. Rev. B **89**, 165307 (2014).
[37] P. B. Ndiaye, C. A. Akosa, M. H. Fischer, A. Vaezi, E.-A. Kim, and A. Manchon, Dirac spin-orbit torques and charge pumping at the surface of topological insulators, Phys. Rev. B **96**, 014408 (2017).
[38] Y. J. Ren, W. Y. Deng, H. Geng, R. Shen, L. B. Shao, L. Sheng, and D. Y. Xing, Spin-orbit torque in a thin film of the topological insulator Bi_2Se_3: Crossover from the ballistic to diffusive regime, Europhys. Lett. **120**, 57004 (2017).
[39] K.-S. Lee, D. Go, A. Manchon, P. M. Haney, M. D. Stiles, H.-W. Lee, and K.-J. Lee, Angular dependence of spin-orbit spin-transfer torques, Phys. Rev. B **91**, 144401 (2015).
[40] K. Garello, I. M. Miron, C. O. Avci, F. Freimuth, Y. Mokrousov, S. Blügel, S. Auffret, O. Boulle, G. Gaudin, and P. Gambardella, Symmetry and magnitude of spin-orbit torques in ferromagnetic heterostructures, Nat. Nanotechnol. **8**, 587 (2013).
[41] L. Liu, C.-F. Pai, Y. Li, H. W. Tseng, D. C. Ralph, and R. A. Buhrman, Spin-torque switching with the giant spin Hall effect of Tantalum, Science **336**, 555 (2012).
[42] R. S. Akzyanov and A. L. Rakhmanov, Surface charge conductivity of a topological insulator in a magnetic field: The effect of hexagonal warping, Phys. Rev. B **97**, 075421 (2018).
[43] R. S. Akzyanov and A. L. Rakhmanov, Bulk and surface spin conductivity in topological insulators with hexagonal warping, Phys. Rev. B **99**, 045436 (2019).
[44] Y. L. Chen, J. G. Analytis, J.-H. Chu, Z. K. Liu, S.-K. Mo, X. L. Qi, H. J. Zhang, D. H. Lu, X. Dai, Z. Fang, S. C. Zhang, I. R. Fisher, Z. Hussain, and Z.-X. Shen, Experimental realization of a three-dimensional topological insulator, Bi_2Te_3, Science **325**, 178 (2009).
[45] D. Hsieh, Y. Xia, L. Wray, D. Qian, A. Pal, J. H. Dil, J. Osterwalder, F. Meier, G. Bihlmayer, C. L. Kane, Y. S. Hor, R. J. Cava, and M. Z. Hasan, Observation of unconventional quantum spin textures in topological insulators, Science **323**, 919 (2009).
[46] C. M. Wang and F. J. Yu, Effects of hexagonal warping on surface transport in topological insulators, Phys. Rev. B **84**, 155440 (2011).
[47] Z.-M. Yu, D.-S. Ma, H. Pan, and Y. Yao, Double reflection and tunneling resonance in a topological insulator: Towards the quantification of warping strength by transport, Phys. Rev. B **96**, 125152 (2017).
[48] Z. Li, and J. P. Carbotte, Hexagonal warping on optical conductivity of surface states in topological insulator Bi_2Te_3, Phys. Rev. B **87**, 155416 (2013).
[49] X. Xiao and W. Wen, Optical conductivities and signatures of topological insulators with hexagonal warping, Phys. Rev. B **88**, 045442 (2013).
[50] Z. Li, and J. P. Carbotte, Hexagonal warping on spin texture, Hall conductivity, and circular dichroism of topological insulators, Phys. Rev. B **89**, 165420 (2014).
[51] L. Fu, Hexagonal Warping Effects in the Surface States of the Topological Insulator Bi_2Te_3, Phys. Rev. Lett. **103**, 266801 (2009).
[52] A. A. Zyuzin, M. D. Hook, and A. A. Burkov, Parallel magnetic field driven quantum phase transition in a thin topological insulator film, Phys. Rev. B **83**, 245428 (2011).
[53] A. Dyrdał, J. Barnaś, and V. K. Dugaev, Current-induced spin polarization of a magnetized two-dimensional electron gas with Rashba spin-orbit interaction, Phys. Rev. B **95**, 245302 (2017).
[54] G. D. Mahan, *Many Particle Physics* (Kluwer Academic, Plenum Publishers, New York, 2000).
[55] N. A. Sinitsyn, J. E. Hill, H. Min, J. Sinova, and A. H. MacDonald, Charge and Spin Hall Conductivity in Metallic Graphene, Phys. Rev. Lett. **97**, 106804 (2006).
[56] N. A. Sinitsyn, A. H. MacDonald, T. Jungwirth, V. K. Dugaev, and J. Sinova, Anomalous Hall effect in a two-dimensional Dirac band: The link between the Kubo-Streda formula and the semiclassical Boltzmann equation approach, Phys. Rev. B **75**, 045315 (2007).
[57] Y.-Y. Yang, M.-X. Deng, W. Luo, R. Ma, S.-H. Zheng, and R.-Q. Wang, Anomalous Nernst effect on a magnetically doped topological insulator surface: A Green's function approach, Phys. Rev. B **98**, 235152 (2018).
[58] See Supplemental Material at http://link.aps.org/supplemental/10.1103/PhysRevB.99.155139 for details of the calculation of spin polarization, vertex correction, and self-energy in the FM/TI bilayer with hexagonal warping.